ELSEVIER

Ceramics International 31 (2005) 929–935

CERAMICS INTERNATIONAL

www.elsevier.com/locate/ceramint

Preparation of ceria–zirconia and yttria–zirconia mixed oxides of unusual pore structures

Michael A. Morris[a,b,*], Helen M. Reidy[a]

[a]*Dimensional Solids Group, University College Cork, Cork, Ireland*
[b]*Centre for Adaptive Nanostructures and Nanodevices, Trinity College Dublin, Dublin, Ireland*

Received 1 September 2004; received in revised form 21 September 2004; accepted 14 October 2004
Available online 13 January 2005

Abstract

Highly ordered particulate assemblies of mixed CeO_2–ZrO_2 and Y_2O_3–ZrO_2 materials have been prepared using a gel-synthesis method. The majority of the particles observed have very regular shapes consisting of sandwiches of parallel pores perpendicular to layers of denser layers. These appear to form from polymeric units of hydrolysed zirconium precursors which facilitate directional growth of the macroscopic moieties. Detailed adsorption experiments and electron microscopy show that two types of pore systems exist in these materials with sizes below 10 nm together with larger more macroscopic pores of the order of 100 nm. The preparation is sensitive to the conditions used in synthesis.

Keywords: D. Ceria; D. Yttria; D. Zirconia; Doped-zirconia; Porous; Ordered macroporous

1. Introduction

Zirconia is a polymorphic oxide exhibiting cubic, monoclinic, tetragonal and orthorhombic distortions of the oxide fluorite arrangement [1]. Doping zirconia with other cations can stabilise the cubic and tetragonal phases by de-stabilising the monoclinic phase [2]. The structural chemistry is also complex in these solid solutions with three different tetragonal phases being observed although these are difficult to resolve by X-ray diffraction and requires analysis by methods such as Raman spectroscopy [3].

Yuan et al. have shown that unusually structured particles of zirconia can be synthesised using a surfactant assisted hydrolysis of zirconium isopropoxide approach [4]. The as-synthesised products have an unusual combination of ordered macropores of diameter 300–500 nm together with a disordered mesoporous structure. The authors argue that supermicelles formed in the reaction conditions result in the development of the macroporous structure. The work presented here extends this synthesis by preparing doped-zirconias and examining these samples after being calcined at high temperatures. In particular, we show that highly thermally stable mixed oxide, macrostructured, porous materials can be produced in the absence of surfactant templates.

2. Experimental

The samples were prepared following a similar route to the method of Rossignol et al. [5]. An appropriate concentration of cerium nitrate was prepared and zirconium or yttrium *n*-propoxide was added drop wise whilst vigorously stirring. A fine white precipitate was formed and the mixture was stirred for 10–30 min to form a suspension. The entire mixture was dried overnight to a solid at 333 K. This is also similar to the method used by Yuan et al. except that their product solution was subjected to a 333 K autoclave treatment for 48 h and their reaction mixture contained a surfactant above its' critical micelle concentration [4]. The relative amounts of materials present

* Corresponding author. Tel.: +353 21 490 2180; fax: +353 21 427 4097.
E-mail address: m.morris@ucc.ie (M.A. Morris).

0272-8842/$30.00
doi:10.1016/j.ceramint.2004.10.006

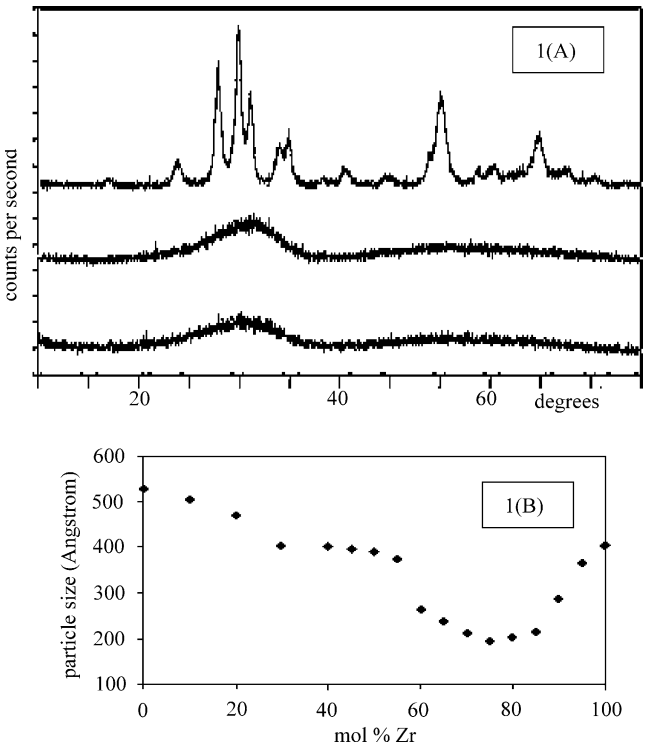

Fig. 1. Panel A shows illustrative PXRD data for a 100% ZrO_2 sample at various calcination times (lower trace = dried at 350 K, middle at 573 K and upper at 1273 K). Panel B shows PXRD-derived crystallite sizes for 873 K calcined materials against zirconia content (mol%).

are given as cation mol% as anion content is very difficult to quantify due to the complex defect chemistry of these oxides. Samples were calcined in air and unless specifically stated the calcination period was 4 h. The bulk structural chemistry was analysed by Powder X-ray Diffraction (PXRD) after calcination at various temperatures and age times. PXRD data was collected on a Phillips PW 3710 MPD instrument, using Cu Kα radiation of wavelength 1.54 Å, with an accelerating voltage of 40 kV and an anode current of 30 mA. Data were collected between 10–70° (2θ), using a step size of 0.03°. Lattice parameters were obtained from Rietveld simulation studies using the Phillips Analytical Rietveld 1.0b software package. This also permitted quantitative analysis of each phase present. Crystallite size was calculated using the Scherrer equation and sizes quoted are an average result of five different reflections. Nitrogen sorption at liquid nitrogen temperature BET measurements were carried out on a Micromeritics Gemini 2375 instrument. BJH data were calculated from the desorption part of the adsorption isotherm. Samples were degassed at 200 °C for 6 h prior to analysis. Secondary electron microscopy data were collected on a Joel Scanning Microscope 35 (JSM-35), using an accelerating voltage of 15 kV. Ground samples were mounted directly onto aluminium stubs using carbon sticky tape and then were sputter coated with gold to ensure adequate electronic conduction.

3. Results

The as-prepared ceria, ceria–zirconia or yttria-ceria materials exhibited negligible mesoporosity as demonstrated by PXRD which showed no sign of a reflection at angles below 10° 2θ. Poorly ordered mesoporosity was demonstrated by 100% zirconia samples only. All traces of mesoporosity as evidenced by PXRD were removed on calcination to 873 K for 4 h. The as-synthesised materials produced were X-ray amorphous until calcinations of 873 K when relatively broad diffraction features were obtained. Illustrative data for 100% ZrO_2 are shown in Fig. 1A. The particle size of the calcined products (at any particular temperature) was strongly dependent on the relative amount of ceria/zirconia present. At any temperature investigated it was found that the smallest particle sizes and broader PXRD features were always observed at around 75 mol% Zr. Typical particle size data are shown in Fig. 1B for samples calcined at 873 K.

As might be expected, the structural phase of the solid mixtures is complex. Following calcination at 1273 K (below this temperature the broadness of the PXRD features

Table 1
Rietveld cell parameters obtained after aging samples at 1273 k for 48 h

Zr mol%	Phases	Fitted lattice parameters			Quantitative analysis (%)
95	T_{Zr}	3.6155	3.6150	5.2085	100
90	T_{Zr}	3.6334	3.6333	5.2284	83.5
	$T_{Zr–Ce}$	3.7843	3.7919	5.0664	16.5
85	T_{Zr}	3.6375	3.6387	5.2364	76.0
	$T_{Zr–Ce}$	3.7717	3.7887	5.3779	24.0
80	T_{Zr}	3.6402	3.6415	5.2395	61.8
	$T_{Zr–Ce}$	3.7797	3.7862	5.3898	38.2
75	T_{Zr}	3.6413	3.6417	5.2393	47.5
	$T_{Zr–Ce}$	3.7742	3.7845	5.3810	52.5
70	T_{Zr}	3.6492	3.6469	5.2446	40.2
	$T_{Zr–Ce}$	3.7820	3.7832	5.3871	59.8
65	T_{Zr}	3.6416	3.6456	5.2447	36.7
	$T_{Zr–Ce}$	3.7834	3.7918	5.3379	63.3
60	T_{Zr}	3.6364	3.6497	5.2299	32.7
	$T_{Zr–Ce}$	3.7859	3.7942	5.3447	67.3
55	T_{Zr}	3.672	3.6563	5.2607	28.7
	$T_{Zr–Ce}$	3.7826	3.7909	5.3243	61.9
	Cubic	5.3826	5.3806	5.3942	9.4
50	T_{Zr}	3.7031	3.6744	5.3247	24.4
	$T_{Zr–Ce}$	3.7932	3.7940	5.3367	62.3
	Cubic	5.4032	5.3929	5.4007	13.3
40	$T_{Zr–Ce}$	3.8123	3.8055	5.4097	85.5
	Cubic	5.4165	5.4066	5.4097	14.5
30	$T_{Zr–Ce}$	3.8090	3.8078	5.3570	77.6
	Cubic	5.4155	5.4082	5.4099	22.4
20	$T_{Zr–Ce}$	3.8209	3.8194	5.2944	54.0
	Cubic	5.4115	5.4074	5.4089	46.0
10	Cubic	5.4120	5.4066	5.4091	100

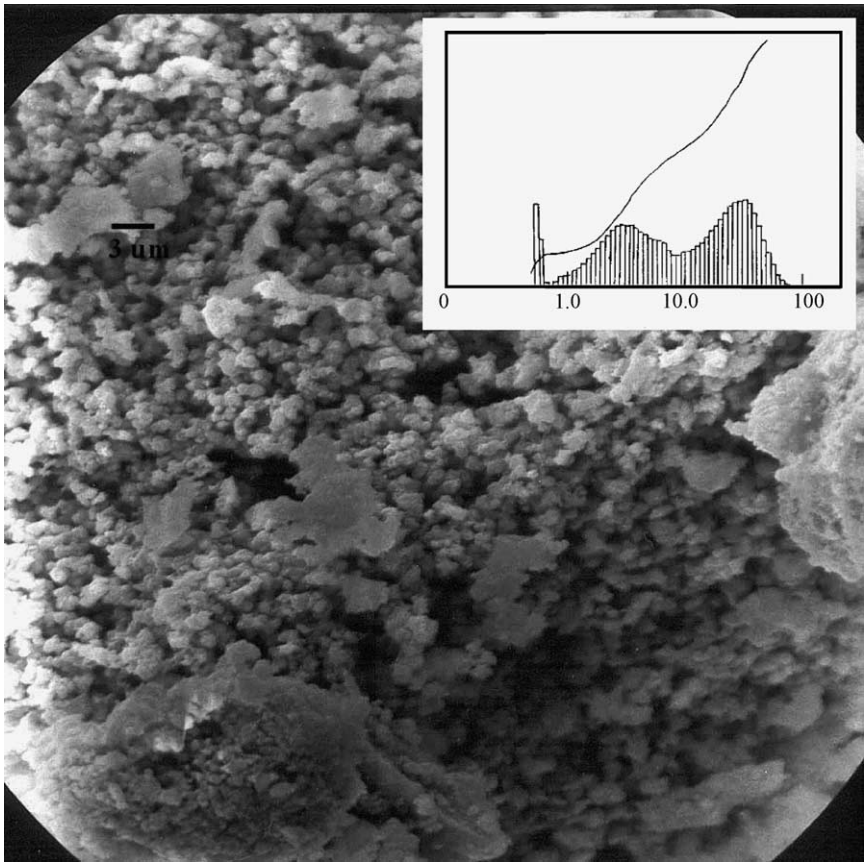

Fig. 2. Main figure is an SEM image of the 75 mol% Zr sample after 873 K calcination showing a bimodal distribution in particle size. The insert is data from light scattering (cumulative undersize vol.% vs. particle size in μm) showing a similar bimodal distribution of particle sizes.

makes quantification of phase impossible using diffraction methods) the zirconia only material exhibited a mixture of tetragonal and monoclinic phases. Addition of 5 mol% cerium stabilised the tetragonal phase and no monoclinic phase was observed. At 10–40 mol% Ce addition two different tetragonal phases were observed. These are labeled as T_{Zr} and $T_{Zr–Ce}$ phases as the T_{Zr} phase is close in structure to that seen for pure zirconia whilst the $T_{Zr–Ce}$ phase shows quite different lattice parameters more typical of a solid solution phase where atom substitution results in lattice parameter changes. The structural parameters are summarised in Table 1. Between 45 and 50 mol% Ce the two tetragonal phases and a cubic phase were observed. Cerium loading above this resulted in the observation of the cubic phase and the $T_{Zr–Ce}$ phase. At cerium concentrations of 90 mol% and above, only the cubic phase is observed. These results are summarised in Table 1 and discussed at length elsewhere [6]. It is clear from these data that the cubic phase of ceria can accept significant amounts of zirconium ions into solid solution. However, the $T_{Zr–Ce}$ phase is largely responsible for the solid solution of mixtures of the cations. The T_{Zr} can only accept a very limited amount of cerium ions into solid solution. In Table 1 the Rietveld-derived phase concentrations show the expected trends of a terminal phase diagram with mixed phases in the centre of the phase diagram and zirconia and ceria-like phases at the high-concentration regions.

SEM and BET surface area data support the PXRD evidence that at around 75 mol% Zr the smallest particle sizes are observed. Typical data are shown in Fig. 2 for samples calcined at 873 K. Around the 75 mol% composition two different particle size regimes appear to be present—the particles have irregular shapes and appear to be made up of assemblies of smaller particles around 0.3 μm. Also present are some larger particles of 12–18 μm in length. This bimodal distribution of particle size is always observed between 65 and 90 mol% Zr and typical size distribution as measured by light scattering data are also shown in Fig. 2. The surface area of calcined materials is relatively small. At higher or lower loadings of zirconia, the particle sizes by SEM or light scattering size analysis increase. This is consistent with the

Table 2
BET-derived surface area measurements for 573 K calcined samples

Zr content (mol%)	Surface area ($m^2\ g^{-1}$)
25	93.7
50	92.6
75	114.3
90	96.3
100	94.2

Table 3
BJH-derived pore volume and surface area estimates (75 mol% Zr materials)

Sample treatment (temperature (K)/time (h))	573/4	773/4	973/4	1173/4	1273/4	1273/48
Surface area ($m^2\ g^{-1}$)	114.3	47.1	41.4	24.2	23.2	16.1
Pore volume below 10 nm ($cm^3\ g^{-1}$)	0.126	0.068	0.049	0.011	0.0026	0.0021
Pore volume 10–100 nm ($cm^3\ g^{-1}$)	0.015	0.003	0.021	0.045	0.038	0.023
Pore volume 0–100 nm	0.141	0.071	0.07	0.046	0.041	0.025

XRD-derived particle size in Fig. 1B. As might be expected from smaller particles, a higher value for the BET estimated surface area data is obtained. Indicative BET results are detailed in Tables 2 and 3. The surface area of samples prepared here is not particularly high (e.g. Stark et al. have observed values of up to 90 $m^2\ g^{-1}$ following calcination at 1173 K [7]). However, even following calcination in severe conditions (1273 K for 48 h) the 75 mol% Zr materials retained surface areas between 15 and 20 $m^2\ g^{-1}$ (for other compositions values decreased to below 10 $m^2\ g^{-1}$).

BET-derived BJH plots can be used to examine the effects of calcination on the porosity of the sample. These data together with surface area values are shown in Table 3 for the 75 mol% Zr materials after various heat and time treatments. 1273 K temperatures are followed over extended periods since this seems to be an important treatment temperature. As might be expected the volume of meso- and micro-pores (i.e. below 10 nm) continuously decreases with calcination temperature. The largest decrease occurs between calcination temperatures of 573 and 773 K as might be predicted by the change in surface area. However, at calcination temperatures of 973 and 1173 K, there is an increase in the volume of larger pores (>10 nm) which then decreases relatively slowly on further calcination (for time or temperature increases). This increase in the volume of large pore diameters compensates for the rapidly decreasing volume of small pores (<10 nm) and this explains why surface area is maintained at reasonably high values even following severe calcinations of 1273 K for 48 h. It is clear that dramatic changes are occurring in the structure of the solid at calcination temperatures around 1000 K.

Evidence for distinct structural rearrangement of the materials is provided by high-resolution electron microscopy work. The unusual particle structures observed by SEM (described in detail below) coincide with calcination temperatures of 1273 K where PXRD data suggest that the crystallisation process becomes rapid. Table 4 shows Scherrer-derived crystallite sizes as a function of heat treatment for a 75 mol% Zr material. These data show that it is only at temperatures around 1273 K that rapid increase in the crystallite size is observed. Following calcinations at this temperature the appearance of unusual complex monolithic morphologies becomes apparent. This structure is most obvious in samples calcined for 48 h and with a Zr content = 75 mol% and is shown in Fig. 3A. The images observed are very similar to those reported by Yuan et al. for as-synthesised (uncalcined) using a cetyltrimethyl ammonium bromide structural directing agent (template) [4]. The calcined materials reported here have well defined reticular parallelpiped morphologies with columnar – almost vertical – macropore channels running from one or sandwiched between two denser planar surfaces (Fig. 3A). This structure will be referred to as rectangular for simplicity even though this is not a truly accurate description. The upper and lower surfaces are not truly dense but rather show large pore openings of 0.5–1 μm in diameter which probably arise from penetration of the macropore channels formed by the columnar structures between the sheets (Fig. 3B). At higher magnification, the dense sheets are also seen to be porous with pore sizes of 80–100 nm and this structure seems to arise from sintering of small particles. These rectangular structures are, on initial comparison, similar to those reported by Yuan et al. [4]. However, the evidence for sintering in the structure reveals an important difference as it clearly results from a very high-temperature treatment that brings about densification and not a low temperature process as used by Yuan et al. [4]. This is confirmed as (unlike the materials described by Yuan et al. [4]) there is only limited amounts of meso- and micro-pores present in these monolithic structures and the data presented in Table 2 and TEM (Fig. 3D) shows no indication of regular or wormhole type structures of sizes in the meso regime.

Table 4
Crystallite size (as derived by PXRD peak broadening) for 75 mol% Zr as function of heat treatment

Sample treatment (temperature (K)/time (h))	Crystallite size (nm)
873/4	6.8
1073/4	6.9
1273/8	16.6
1273/12	18.6
1273/24	21.3
1273/48	24.9

It should be noted that these unusual particle morphologies are very common in these preparations. Nearly all the mixed materials (between 30 and 90 mol% Zr) prepared here exhibit similar structures following these aggressive calcinations. However, 75 mol% Zr appears to be an optimum composition and this produced samples in which over 70% of all particles had these unusual morphologies from many different repeat synthesis.

There is distinct compositional variation across these monolithic structures. Detailed EDAX measurements were made by measuring the relative intensity of the Ce to Zr Kα fluorescent peaks for the 75 mol% Zr samples. Comparison was made to a series of standards prepared by thermal fusion

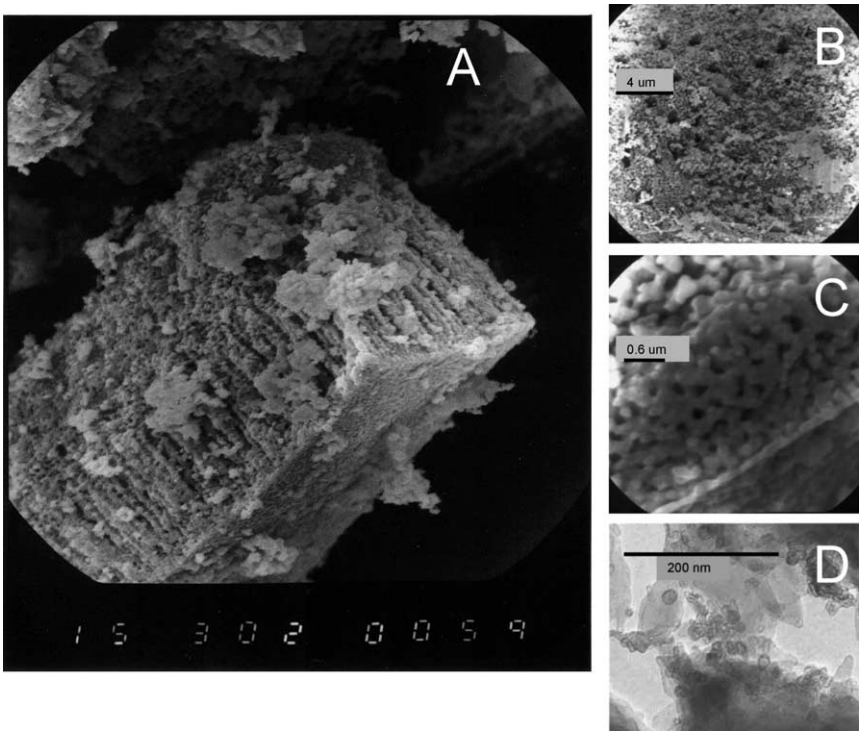

Fig. 3. SEM data (magnification 30×10^2) of unusual particle morphology after high-temperature calcination (A). Image from the flat surface of these rectangular particles showing the macropore openings at the surface (B). Higher magnification shows the porous nature of the flat surfaces (C). High-resolution transmission electron microscopy (TEM) reveals no meso- or micro-pore structure (D).

of ceria and zirconia powders. This showed that the columnar structure has a cerium content of 35–38 mol% Ce whilst the denser layers had zirconium concentrations of 95–98 mol% Zr. Comparing to the data above this would suggest that the columnar structure has a mixture of the T_{Zr} and $T_{Zr–Ce}$ structures present whilst the layers have a T_{Zr} structure. This phase separation was observed in all the structures shown here.

It is interesting to note that these structures were only observed in acid conditions. The solution of the reaction used here has a pH of 4. The reaction was repeated using a 1 M NH_4OH solution to adjust the pH of the solutions to 8 and 12. A distinct change in behaviour was observed and in alkaline conditions the as-synthesised products were much more crystalline in nature. Typical PXRD data illustrating this behaviour for as-synthesised filtered materials (75 mol% Zr) are shown in Fig. 4. It is of interest to note that no unusual monolithic structures were observed for the base conditions.

It should be stressed that these structures are not unique to ceria–zirconia mixtures. Similar unusual monolithic macroporous structures were observed in the preparation of yttria–zirconia mixed oxides. In the case of yttria materials the optimum concentration of yttrium was 4 mol% rather than the 25 mol% for cerium doping. Typical electron micrographs are shown in Fig. 5. The rectangular arrangements are dominant in the particles observed but for the yttria–zirconia materials several examples of screw arrangements of the sandwich structure were apparent. The ‘pores’ are also somewhat smaller than for ceria-doped materials and analysis of the electron microscopy data suggest sizes of between 400 and 600 nm.

4. Discussion

The monolithic macroporous particle morphologies observed here are highly novel. They are similar to structures previously reported [4] except that they were not observed in as-synthesised materials but were only seen for materials calcined at the most robust temperatures. Yuan

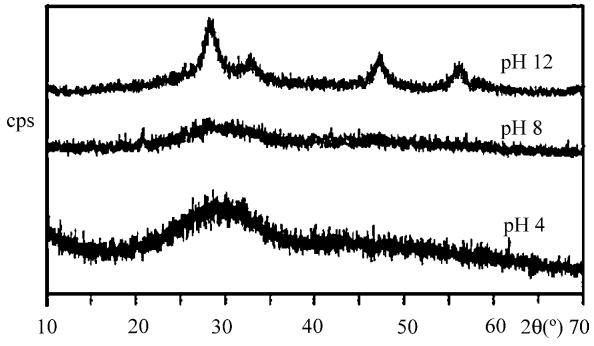

Fig. 4. Variation of the PXRD data observed as a function of pH during synthesis of a ceria–zirconia material (75 mol% Zr). From top to bottom pH 12, 8 and 4 are shown.

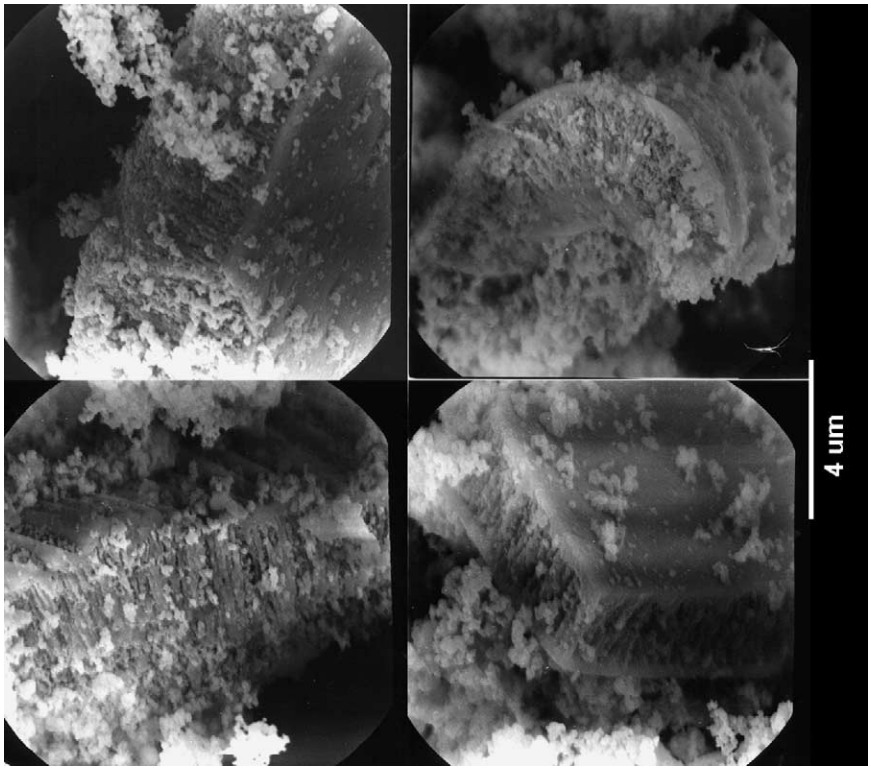

Fig. 5. SEM data of particle morphology from yttria–zirconia (65 mol% Zr) materials. The upper images and bottom left are the more common rectangular arrangements but screw-like arrangements are also observed (bottom right).

et al. have suggested that the structures they are observed arose from a complex structural directing property of added surfactant micelles [4]. This is not possible for our materials as no surfactants are added. We suggest that it is the ability of zirconium *n*-propoxide to exist as small polymer units in its own alcohol and a tendency to hydrolyse/condense into polymer chains [8] that is at least partly responsible for the unusual monolithic structures observed here. We do not believe that these zirconium *n*-propoxide polymers could form micelles and so 'template' the products in the way proposed by Yuan et al. [4]. We have seen no evidence to support surfactant micelle formation in aqueous solutions containing more than 1–2% propanol. We believe that the polymerisation of the propoxide coupled to the reaction conditions results in linear aggregations of material. As discussed by Orcel et al. reaction conditions can strongly influence the shape of polymeric units formed by hydrolysis-condensation reactions [9]. In particular, these authors showed that fast hydrolysis and slow condensation yielded linear polymer units whilst the reverse conditions favoured larger and bulkier more ramified units. Since acid conditions favour hydrolysis and base favours condensation processes, it is clear our conditions favour more linear structures. These theories are supported by some of the work reported here; note how moving from acid to base conditions produces as-synthesised materials with much more highly organised crystalline structures (Fig. 4).

We believe that the propoxide polymer units hydrolyse to form distinct linear chains of general structure:

$$\begin{array}{c} OH_2^+ \quad OH_2^+ \\ | \quad\quad | \\ RO\,(-Zr-O-Zr-)_n\,OR \\ | \quad\quad | \\ OH_2^+ \quad OH_2^+ \end{array}$$

This is because the protonated species $(OR)_2Zr(OH_2^+)_2$ predominates in acid conditions [10]. Cross-linking across the $Zr\text{-}OH_2^+$ units is less likely than across Z-OR units and so elongated primary particles are observed. It appears that cerium ions have an important role to play in these reactions; this may be by simply adjusting the pH of the solutions or by controlling the rates of cross-linking and chain extension reactions. These elongated primary particles may be assembled into larger secondary particles. However, the sheaf of charge from the OH_2^+ species limits complete 3D densification and eventually leads to the columnar structures observed. The denser sheet-like parts of the structures are formed by assembly of more regularly shaped entities.

As mentioned above, cerium ions play an important role. This, we believe, is because crystallisation and phase separation play important roles in the formation of the monolithic structure. The X-ray analysis results suggest that phase separation exists between the base and columns of the monolith. This may be because ceria preferentially favours the 2D growth and so gives the elongated particles used to form the columnar structure. The zirconia rich particles are

more regular and sinter to give the sheet-like structures. There is little sign of the monolithic macropore structures being formed at lower temperatures. The observation of these structures at only high-temperature calcination suggests that they are only formed during crystallisation and the densification separates the extended polymer-like entities into well-separated columnar structures. It may be that in the work of Yuan et al. [4] that the surfactants did interact with the chains to create wide separation distances in the as-synthesised material.

5. Concluding remarks

The observation of these unusual monolithic structures is interesting. There are also a number of important applications of these materials. In catalysis (particularly high-temperature zirconia catalysis) attainment and maintenance of surface area is obviously desirable. However, ease of accessibility of the surface is also of importance, i.e. non-torturous pore systems that can be accessed with low pressure drop. It is asserted here that these materials do have unexpectedly high surface areas even after very severe thermal treatments and also demonstrate very high pore volumes. These couple to provide what might be very effective contact dynamics in practical catalytic applications. These materials might have important applications in exhaust catalysis and fuel cells.

References

[1] R.C. Garvie, J. Phys. Chem. 69 (1965) 1238;
R.C. Garvie, J. Phys. Chem. 82 (1978) 218.
[2] A.P. Bechepeche, O. Treu Jr., E. Longo, C.O. Paiva-Santos, J.A. Varela, J. Mater. Sci. 34 (1999) 2751.
[3] M. Yashima, H. Arashi, M. Kakihana, M. Yoshimura, J. Am. Ceram. Soc. 77 (1994) 1067.
[4] Z.-Y. Yuan, A. Vantomme, A. Léonard, B.-L. Su, Chem. Commun. (2003) 1558.
[5] S. Rossignol, Y. Madier, D. Duprez, Catal. Today 50 (1999) 261.
[6] H. Reidy, M.A. Morris, J. Am. Ceram. Soc., submitted for publication; H. Reidy, PhD Thesis, University College Cork, Cork, Ireland.
[7] W.J. Stark, M. Maciejewski, L. Mädler, S.E. Pratsinis, A. Baiker, J. Catal. 220 (2003) 35.
[8] K. Yamashita, T. Kanazawa, in: T. Kanazawa (Ed.), Inorganic Phosphate Materials, Kodansha, Tokyo, 1989.
[9] G. Orcel, L.L. Hench, I. Artaki, J. Jones, T.W. Zerda, J. Non-Cryst. Solids 105 (1988) 223.
[10] G.K. Chuah, S.H. Liu, S. Jaenicke, J. Li, Microporous Mesoporous Mater. 39 (2000) 381.